ARTICLES

Transition State Dynamics of Ar_n·(IHI) ($n = 0-20$)

José G. López and Anne B. McCoy*

Department of Chemistry, The Ohio State University, Columbus, Ohio 43210

Received: September 13, 2004; In Final Form: November 12, 2004

Classical trajectory simulations of the dynamics of Ar_n·(IHI) with $n = 0-20$ are performed to investigate the effects of solvation on the transition state dynamics of the I + HI reaction. Initial conditions for the classical trajectories are sampled from the quantum ground-state phase space distribution for Ar_n·$(IHI)^-$, given by the Wigner distribution function. Neumark and co-workers recently reported a shift of the Ar_n·$(IHI)^-$ photoelectron spectra to lower electron kinetic energies when the number of argon atoms was increased from 0 to 15. Analogous shifts are found in the present calculations, and excellent agreement between the experimental and calculated shifts is found. Longer lifetimes of the IHI complex and increasing energy transfer between the hydrogen atom and the argon and iodine atoms are also observed as the number of argon atoms is increased.

Introduction

The transition state of a chemical reaction is given a special place in the description of reaction dynamics.[1] One powerful way to investigate how a solvent can affect a chemical reaction is through studies that focus on this region of the potential. Several experimental techniques have been applied to studies of the transition state.[2−4] Among them, negative ion photodetachment experiments have proven to be particularly fruitful. In these experiments, electron photodetachment of a stable anion is used to reach the transition state region of the reaction of interest, and the distribution of the electron kinetic energies provides a probe of the transition state resonance structure for the reaction on the corresponding neutral potential surface.[5]

In the present study we investigate the effects of the introduction of argon atoms on the transition state dynamics of the I + HI reaction. Our primary motivation for studying this system comes from the recent experimental investigations of Newmark and co-workers, in which they measured the photoelectron (PE) spectra of Ar_n·$(IHI)^-$ with $n = 0-15$.[6−8] We are also interested in developing the theoretical and computational tools that are required to investigate the dynamics of weakly bound systems.

Over the past decade Neumark and co-workers have applied anion photodetachment techniques to studies of bimolecular reactions of the type X + HY → XH + Y, where X and Y are halogen atoms.[5,6,9−11] For the $(XHX)^-$ (X = Br, Cl, and I) and $(BrHI)^-$ complexes, a strong progression in the antisymmetric stretch (ν_3) of the corresponding neutral complex was observed.[6,10,11] More recently, they investigated the effects of introducing argon atoms on the transition state region of these reactions.[7,8] When one argon atom was added, they found a shift of the $(IHI)^-$ and $(BrHI)^-$ PE spectra to lower electron kinetic energies.[7] The introduction of additional argon atoms to the $(IHI)^-$ complex led to a shift to still lower electron kinetic energies.[8] This shift was interpreted to reflect a greater stabilization of the anion, relative to the neutral complex, by the argon atoms. In addition, the Ar·$(IHI)^-$ PE spectrum showed weak progressions that reflected transitions to hinder rotor levels of the hydrogen in the IHI complex. Interestingly, this structure became more pronounced for the largest Ar_n·$(IHI)^-$ clusters that were investigated in that study. This was attributed to a longer lifetime of the unbound IHI complex due to a caging of the hydrogen atom by the argon atoms.[12]

Photodetachment of $(XHY)^-$ bihalide anions have also been of interest from a theoretical point of view,[13−23] and several studies of the dynamics of Ar_n·$(ClHCl)^-$ have been performed in our group.[24−26] Our interest in these systems has derived from our desire to identify appropriate computational approaches that will allow us to gain physical insights into the XHX transition state dynamics and study the effects of solvating atoms on the dynamics.

In this work, we report the results of classical trajectory studies of the transition state dynamics of the Ar_n·(IHI) complex with $n = 0-20$. We focus on the following two issues. First, how do the argon atoms cluster around the $(IHI)^-$ and how do they perturb its geometry. Second, how does the introduction of argon atoms affect the time evolution of IHI.

Although the presence of a hydrogen atom leads us to expect that quantum effects will be important, we select a classical methodology to simulate the evolution of Ar_n·(IHI) because it will provide us with physical insights into the dynamics of the system in a way that is less computationally demanding than a quantum calculation, as well as the extent to which classical mechanics can be used to describe the dynamics of the Ar_n·(IHI) complexes. This will help us to develop appropriate approximate quantum approaches for future studies of the transition state spectroscopy and dynamics of weakly bound complexes.

Theory

A. Coordinates and Hamiltonian. For the classical trajectory simulations of Ar_n·(IHI) we use Cartesian coordinates. For N atoms the classical Hamiltonian in Cartesian coordinates is

$$H = \sum_{i=1}^{3N} \frac{p_i^2}{2m_i} + V(\mathbf{x}) \tag{1}$$

where p_i represents the ith Cartesian component of the $3N$

10.1021/jp045862r CCC: $30.25
Published on Web 01/27/2005

dimensional momentum vector, m_i provides the mass of the associated atom, **x** represents the Cartesian coordinates of the atoms, and $V(\mathbf{x})$ is the interaction potential.

Simulations of the transition state dynamics of the I + HI reaction require potential energy surfaces for Ar_n·$(IHI)^-$ and Ar_n·(IHI). In this work, the Ar_n·$(IHI)^-$ intermolecular potential is given by

$$V^{\text{inter}}_{\text{Ar}_n\cdot(\text{IHI})} = \sum_{i=1}^{n}\{F(r_1,r_2)[V_{\text{Ar-IH}}(R_{\text{Ar}_i\text{I}_1},\theta_{\text{HI}_1\text{Ar}_i}) + V_{\text{Ar-I-}}(R_{\text{Ar}_i\text{I}_2})] + [1 - F(r_1,r_2)][V_{\text{Ar-IH}}(R_{\text{Ar}_i\text{I}_2},\theta_{\text{HI}_2\text{Ar}_i}) + V_{\text{Ar-I-}}(R_{\text{Ar}_i\text{I}_1})]\} + \sum_{j>i}^{n} V_{\text{Ar-Ar}}(R_{\text{Ar}_i\text{Ar}_j}) + \sum_{k=1}^{2}\sum_{j>i}^{n} \frac{\mu^{(k)}_{\text{Ar}_i}\mu^{(k)}_{\text{Ar}_j}}{R^3_{\text{Ar}_i\text{Ar}_j}}(2\cos\phi_{ijk}\cos\phi_{jik} + \sin\phi_{ijk}\sin\phi_{jik}) \quad (2)$$

where R_{AB} represents the distance between the atoms A and B, r_1 and r_2 the I_1−H and H−I_2 distances, respectively, $\theta_{\text{HI}_k\text{Ar}_i}$ the H−I_k−Ar_i angle, and ϕ_{ijk} the Ar_i−Ar_j−I_k angle. The first term of eq 2 results from treating two asymptotic cases: Ar_i·(I_1H+I_2^-) and Ar_i·(I_1^-+HI_2). The potentials are combined using a switching function,

$$F(r_1,r_2) = \frac{1 - \tanh[\beta(r_1 - r_2)]}{2} \quad (3)$$

where β is chosen to be 1.0. The Ar−HI potential, $V_{\text{Ar-IH}}$ in eq 2, is given by an ab initio potential[27] whereas the Ar−I^- interaction is represented by a Morse−Morse−switching function−van der Waals potential.[28] $V_{\text{Ar-Ar}}$ represents the Ar−Ar potential. For this potential, we use the Ar−Ar Hartree−Fock-dispersion potential of Aziz and Slaman.[29] The final term represents the argon atoms induced dipole−induced dipole interactions,[30] where

$$\mu_i^{(1)} = -[1 - F(r_1,r_2)]\frac{\alpha_{\text{Ar}}}{R^2_{\text{Ar}_i\text{I}_1}} \quad (4)$$

$$\mu_i^{(2)} = -F(r_1,r_2)\frac{\alpha_{\text{Ar}}}{R^2_{\text{Ar}_i\text{I}_2}} \quad (5)$$

represent the induced dipoles, and α_{Ar} is the polarizability or argon (11.096 a_0^3).[31] Finally, the total potential for Ar_n·$(IHI)^-$ is obtained by adding a harmonic potential for $(IHI)^-$.[32]

The potential for Ar_n·(IHI) is similar to the Ar_n·$(IHI)^-$ potential, except for the removal of the final term of eq 2 and the $(IHI)^-$ harmonic potential is replaced by the LEPS-A potential energy surface for the I+HI reaction of Manz and Römelt.[33] As such, the intermolecular potential for Ar_n·(IHI) is given by

$$V^{\text{inter}}_{\text{Ar}_n\cdot(\text{IHI})} = \sum_{i=1}^{n}\{F(r_1,r_2)[V_{\text{Ar-IH}}(R_{\text{Ar}_i\text{I}_1},\theta_{\text{HI}_1\text{Ar}_i}) + V_{\text{Ar-I}}(R_{\text{Ar}_i\text{I}_2})] + [1 - F(r_1,r_2)][V_{\text{Ar-IH}}(R_{\text{Ar}_i\text{I}_2},\theta_{\text{HI}_2\text{Ar}_i}) + V_{\text{Ar-I}}(R_{\text{Ar}_i\text{I}_1})]\} + \sum_{j>i}^{n} V_{\text{Ar-Ar}}(R_{\text{Ar}_i\text{Ar}_j}) \quad (6)$$

It should be noted that except for β in eq 3 there are not any adjustable parameters in the above empirical potentials.

To facilitate the simulations, we approximate the Ar_n·(IHI) intermolecular potential by a sum of pairwise interactions

$$V^{\text{inter}}_{\text{Ar}_n\cdot(\text{IHI})} = \sum_{i=1}^{n}[V_{\text{Ar-I}}(R_{\text{Ar}_i\text{I}_1}) + V_{\text{Ar-I}}(R_{\text{Ar}_i\text{I}_2}) + V_{\text{Ar-H}}(R_{\text{Ar}_i\text{H}})] + \sum_{j>i}^{n} V_{\text{Ar-Ar}}(R_{\text{Ar}_i\text{Ar}_j}) \quad (7)$$

where the parameters that control the Ar−I and Ar−H interactions are modified to fit the Ar_n·(IHI) intermolecular potential given in eq 6 near the global minimum. In this potential, the Ar−I interaction is represented by a Morse−Morse−switching function−van der Waals potential given in ref 28 and the Ar−H interaction by a Morse potential[24]

$$V(r) = D_e(1 - e^{-\alpha(r-R_e)})^2 \quad (8)$$

The values of the original and modified parameters are listed in Table 1.

B. Determination of Initial Conditions. The initial conditions for the classical trajectory simulations of Ar_n·(IHI) are obtained from the ground-state wave function of Ar_n·$(IHI)^-$, assuming a vertical transition to the Ar_n·(IHI) surface. For the four normal coordinates that describe the $(IHI)^-$ vibrations we sample the initial conditions using the Wigner distribution function[34]

$$W(\mathbf{Q},\mathbf{P}) = \prod_{i=1}^{4} w(Q_i,P_i) \quad (9)$$

where

$$w(Q_i,P_i) = \frac{1}{\pi\hbar}\int_{-\infty}^{\infty} ds\, \exp\left(\frac{-2iP_is}{\hbar}\right)\psi_i^*(Q_i - s)\,\psi_i(Q_i + s) \quad (10)$$

and Q_i and P_i represent each of the normal coordinates and momenta of $(IHI)^-$ and ψ_i is the harmonic ground state wave function for the ith mode of the anion. The normal coordinates are obtained by diagonalizing the matrix of second derivatives of the potential with respect to the mass-weighted Cartesian coordinates, evaluated at the minimum of the potential.[35] Initial conditions in Cartesian coordinates are obtained using the resulting L matrix.

C. Propagation. Once the initial conditions have been determined, the dynamics of Ar_n·(IHI) is propagated by solving Hamilton's equations of motion

$$\frac{\partial H}{\partial p_i} = \dot{x}_i \quad (11)$$

$$\frac{\partial H}{\partial x_i} = -\dot{p}_i \quad (12)$$

for each of the $3N$ Cartesian coordinates and momenta that describe the system. The solution of these equations is implemented using the Gear method.[36]

III. Results and Discussion

A. Minimum Energy Structures for the Ar_n·$(IHI)^-$ Clusters. The equilibrium positions of the argon atoms have been determined using the potential for Ar_n·$(IHI)^-$, described above.

TABLE 1: Original Values for the Parameters in the Ar−I[28] and Ar−H[24] Potentials and the Corresponding Values Used in This Work To Fit the Intermolecular Ar_n·(IHI) Potential Energy Surface Given in Eq 6 into a Sum of Pairwise Potentials As Given in Eq 7

potential	parameter	original value	this work
Ar−I	ϵ (meV)	18.8	16.70
	r_m (Å)	3.95	3.95
	β_1	7.15	6.52
	β_2	6.18	5.61
	x_1	1.01	1.01
	x_1	1.62	1.62
	C_6 (eV Å^6)	98.4	98.4
	C_8 (eV Å^8)	715.	715.
Ar−H	D_e (cm^{-1})	38.717	38.717
	α (Å^{-1})	1.73	1.30
	R_e (Å)	3.56	3.93

For $(IHI)^-$ this potential predicts a linear and centrosymmetric structure, as shown in Figure 1a. Addition of one argon atom results in a T-shape complex. The next five argon atoms cluster around the I−I axis, forming a ring that is perpendicular to this axis with the hydrogen atom at the center of the ring, as is shown in Figure 1b,c. When more argon atoms are introduced, they bind to a single iodine atom forming a second six-membered ring. The 12th argon atom completes this second ring and the 13th one caps the end of the cluster, as shown in panels d and e. The 14th argon atom starts a ring around the other iodine atom. The next five argon atoms form this third ring, whereas the 20th one caps this end of the cluster, completing the first solvation shell for $(IHI)^-$, Figure 1f. Larger complexes were not considered in the present study. Structural parameters for these complexes are reported in Table 2. Comparing the dissociation energies of the Ar_n·$(IHI)^-$ complexes we find that the ones with $n = 6$, 12, and 19 are particularly stable.

Adamovic and Gordon[37] have also studied the structure and energetics of Ar_n·$(IHI)^-$ ($n = 0-7$). They investigated various stationary points on the potential surfaces at the MP2 level of theory, with a aug-cc-pVTZ basis set for the argon atoms, the SBKJC effective core potential for the iodine atoms, and the 6-311++G(2d,2p) basis for the hydrogen atom. They also performed single point CCSD(T) calculations for clusters with three or fewer argon atoms. If we focus on the lowest energy structures, we find that these ab initio calculations show the same clustering patterns and similar Ar−Ar and Ar−H distances as we report in Table 2 and Figure 1.

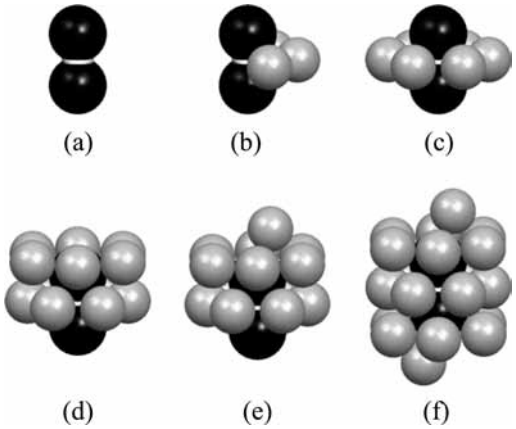

Figure 1. Minimum energy structures of the Ar_n·$(IHI)^-$ clusters for (a) $n = 0$, (b) $n = 3$, (c) $n = 6$, (d) $n = 12$, (e) $n = 13$, and (f) $n = 20$.

The observed clustering pattern is also consistent with the results of our study of the Ar_n·$(ClHCl)^-$ system[26] when $n = 1-3$. In that work we reported symmetric configurations of the argon atoms when $n = 4$ or 5, whereas only six argon atoms form a symmetric ring around $(IHI)^-$. This discrepancy led us to revisit the structures of the Ar_n·$(ClHCl)^-$ clusters. We identified an error in the evaluation of the potential in the earlier studies. When this was corrected, the structure of the Ar_4·$(ClHCl)^-$ complex was no longer symmetric, but the Ar_5·$(ClHCl)^-$ system retained the previously reported structure, with the five argon atoms forming a regular pentagon around the hydrogen atom.

TABLE 2: Minimum Energy Structures and Dissociation Energies for Some Ar_n·$(IHI)^-$ Clusters

parameter	$n = 0$	$n = 1$	$n = 2$	$n = 3$	$n = 4$	$n = 5$	$n = 6$
R_{IH} (Å)	1.9400	1.9402	1.9404	1.9407	1.9410	1.9413	1.9400
R_{ArH} (Å)		3.6375	3.6412	3.6423	3.6453	3.6393	3.6991
				3.6473	3.6479	3.6461	
						3.6439	
θ_{IHI} (deg)	180.00	179.82	179.69	179.65	179.71	179.86	180.00
θ_{ArHAr} (deg)[a]			62.47	62.33	62.30	62.54	60.00
					62.22	62.43	
D_e (cm^{-1})[b]	0.00	512.35	1112.13	1713.81	2315.29	2921.25	3593.94

parameter	$n = 7$	$n = 9$	$n = 12$	$n = 13$	$n = 14$	$n = 19$	$n = 20$
R_{I_1H} (Å)	1.9317	1.9188	1.9013	1.8989	1.9063	1.9332	1.9317
R_{HI_2} (Å)	1.9476	1.9593	1.9736	1.9724	1.9645	1.9329	1.9317
R_{ArI_i} (Å)[c]	4.1175	4.1094	4.0627	4.0608	4.1257	4.0545	4.0612
		4.1101		4.0302		4.0575	4.0275
				4.0745		4.0562	4.0525
				3.9199			3.9212
θ_{IHI} (deg)	179.99	179.96	180.00	179.93	179.95	179.92	180.00
$\theta_{ArI_iI_j}$ (deg)[c]	106.82	106.95	108.30	110.07	105.10	106.59	108.56
		106.08		111.63		106.48	109.49
				110.14		106.62	108.53
				165.16			163.15
θ_{ArI_iAr} (deg)[a,c]		54.91	56.68	55.86		57.56	56.13
				56.21		57.22	56.31
				55.71		57.14	56.75
				55.21		57.37	56.65
D_e (cm^{-1})[b]	4086.22	5258.53	7100.85	7697.24	8193.93	11225.83	11804.63

[a] Only the angles between adjacent argon atoms are reported. [b] $D_e = E(nAr+(IHI)^-) - E(Ar_n\cdot(IHI)^-)$. [c] For $n = 7$, 9, 12, and 13 $i = 2$ and $j = 1$. For $n = 14$, 19, and 20 $i = 1$ and $j = 2$. Only the argon atoms clustering around I_i are considered.

The difference in the number of argon atoms that form a ring around the center of $(XHX)^-$ can be understood in terms of the difference between the radii of chlorine and iodine. As seen in Table 2, when $n = 2-4$, the Ar−H−Ar angle between adjacent argon atoms is consistently 62°, whereas in ClHCl, this angle is roughly 72°. As a result, whereas the symmetric argon ring around $(ClHCl)^-$ contains $360/72 = 5$ argon atoms, in the $(IHI)^-$ complex, the smaller Ar−H−Ar angle results in a stable argon ring that contains six argon atoms. The larger argon ring in the $(IHI)^-$ system is further supported by studies of $Ar_n \cdot I_2^-$,[38,39] which show the same clustering pattern as we described above. Parson and co-workers[38] also reported that particularly stable clusters are found for $n = 6$, 12, 13, 19, and 20.

In addition to the positions of the argon atoms, we studied the effects of the argon atoms on the $(IHI)^-$ geometry through the analysis of the I−I and H−I distances, and the I−H−I angle as functions of the number of argon atoms. These results are reported in Table 2. For $n \leq 5$ we found a slight increase of the interiodine distance. However, for $n = 6$ we found that the I−I distance is equal to its value when no argon atoms are present. For $n > 6$ a successive decrease of the interiodine distance was observed. Finally, the presence of argon atoms causes $(IHI)^-$to bend slightly.

Due to the symmetry of the clusters with $n \leq 6$, the two H−I distances must be equal. This symmetry is broken when more than six argon atoms are introduced and the equivalence of the two H−I distances is lost. For the $n = 7-13$ clusters, the hydrogen atom is closer to the less solvated iodine atom, I_1. We also find a slightly larger negative charge, ranging from 0.016 to 0.074, on the more solvated iodine atom, I_2. This is consistent with previous studies of complexes of I_2^- with Ar[38,40] and CO_2.[41]

B. Solvation Energies for the $Ar_n \cdot (IHI)^-$ and $Ar_n \cdot (IHI)$ Clusters. Due to the stronger interaction of the argon atoms with $(IHI)^-$ than with IHI, each additional argon atom stabilizes the anion more than the neutral cluster. This results in a successive shift of the photoelectron spectra of $Ar_n \cdot (IHI)^-$ to lower electron kinetic energies upon the introduction of each additional argon atom.[8] The stepwise spectral shift is reflected in the shift of the positions of the $\nu_3' = 0$, 2, and 4 bands in the $Ar_n \cdot (IHI)^-$ PE spectrum compared to the $Ar_{n-1} \cdot (IHI)^-$ PE spectrum. The leading contribution to the stepwise spectral shift comes from the difference between the solvation energies of the anion and the neutral complexes, $\Delta E_{solv}(n)$, where we define the solvation energies as the dissociation energy for the loss of a single argon atom from $Ar_n \cdot (IHI)^-$ or $Ar_n \cdot (IHI)$.[8] Because these solvation energies depend on the positions of the argon atoms, one way to obtain experimental evidence of the structure of the complexes is to compare the experimental stepwise spectral shifts and the calculated $\Delta E_{solv}(n)$. The results of such a comparison are plotted in Figure 2, where the experimental stepwise shifts for the $\nu_3' = 2$ peak are plotted with white squares and the calculated $\Delta E_{solv}(n)$ values with black circles. Neumark and co-workers also reported the stepwise spectral shifts for the $\nu_3' = 0$ and 4 bands, where similar trends are observed. Although the calculated $\Delta E_{solv}(n)$ values do not include quantum effects such as changes in the vibrational frequencies of IHI or $(IHI)^-$ upon solvation, they are able to pick up the overall trends in the experimental curve. This similarity, along with the good agreement with the anion geometrical structures obtained by Adamovic and Gordon,[37] suggests that our potential energy surfaces capture the essential physics of the complexes.

Although the general structures of the two curves in Figure 2 are in good agreement, there are notable differences. For the first six argon atoms the calculated $\Delta E_{solv}(n)$ decreases slightly, whereas the experimental results remain nearly constant. However, for $n = 7$ significant reductions in both the experimental and calculated $\Delta E_{solv}(n)$ are observed. This large drop in the stepwise spectral shift has been interpreted to reflect a change in the clustering position of the seventh argon atom,[8] compared to the first six. As we mentioned above, though the first six argon atoms cluster around the hydrogen atom, the seventh argon atom binds to a single iodine atom, resulting in a weaker overall Ar−I interaction energy, and therefore, in a reduction of the stepwise spectral shift.

For $n = 7-15$ quantitative agreement between the calculated and experimental results is achieved, including the drop for $n = 12$ and 13. This drop is, at first glance, somewhat surprising as the 12th and 13th argon atoms bind in different locations, as shown in Figure 1. Examination of Figure 3 shows that the contributions to the stepwise solvation energies for the anion and neutral change rapidly over this range of cluster sizes, and the near agreement of the stepwise spectral shifts for the $n = 12$ and 13 reflect different properties of these potentials and provide a stringent test of the potential surfaces used in the study.

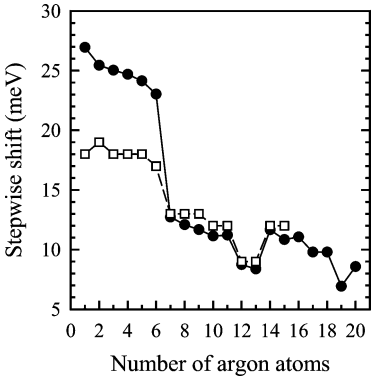

Figure 2. Plots of the calculated $\Delta E_{solv}(n)$ values (black circles) and the experimental stepwise spectral shifts (white squares) for the $\nu_3' = 2$ peak as functions of the number of argon atoms in the system. In the experimental stepwise shifts, because spectra for $n = 8$, 10, 12, and 14 were not recorded, the values for $n = 8-15$ were taken to be equal to half the shift between n and $n - 2$.[8]

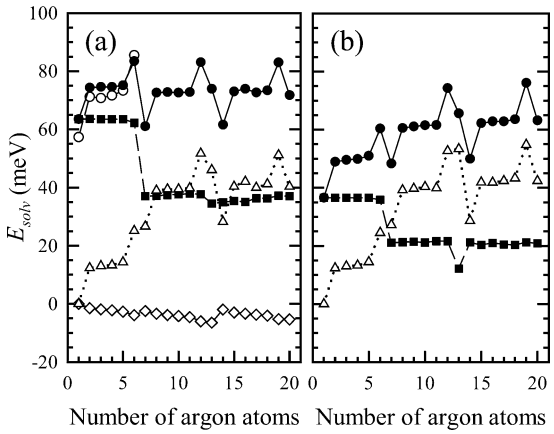

Figure 3. Stepwise solvation energies (black circles) for (a) $Ar_n \cdot (IHI)^-$ and (b) $Ar_n \cdot (IHI)$, plotted as a function of the number of argon atoms in the system. The Ar−$(IHI)^-$ or Ar−(IHI) contributions are plotted with black squares. The Ar−Ar contribution is indicated by white triangles and the induced dipole−induced dipole contribution is plotted with white diamonds. The white circles represent the stepwise solvation energies for the anion, calculated by Adamovic and Gordon.[37]

For $n \leq 6$ larger differences are found. To investigate this discrepancy, we analyze the contributions to the stepwise solvation energies for both the anion and the neutral complexes. The results are plotted in Figure 3. In the case of the anion, we also compare our binding energies with the MP2 energies reported by Adamovic and Gordon.[37] For $n \leq 6$ these plots show that the Ar−Ar interactions make similar contributions to the energies of the anion and neutral. Though the Ar−Ar interactions for the anion also include a three-body induced dipole−induced dipole term, it contributes less than 5 meV to the total energy. Because $\Delta E_{solv}(n)$ is defined as the difference between the anion and neutral stepwise solvation energies, the above terms introduce only a small contribution and for $n \leq 6$ the largest contribution comes from the interaction between the argon atoms and $(IHI)^-$ or IHI. From the plots in Figure 3 we find that the difference between the stepwise solvation energies of the anion and neutral is roughly 27 meV and is nearly constant for $n = 1-5$.

Although the calculated stepwise solvation energies for the anion follow the same trend as those calculated by Adamovic and Gordon, a quantitative comparison reveals a difference of about 6 meV for $n = 1$ and 3 meV for $n = 2-4$. In addition, for $n = 1$, comparisons with the binding energy of $Ar\cdot(IHI)^-$, determined by Neumark and co-workers,[7] show that the present empirical potentials overestimate this quantity by about 10 meV. From this comparison, it is likely that our $Ar\cdot(IHI)^-$ interaction energies are slightly too large. We have investigated how scaling this term affects $\Delta E_{solv}(n)$. We found that it has a larger effect on $\Delta E_{solv}(n)$ for $n \leq 6$ than for larger complexes. This leads us to expect that such a scaling will enable us to bring our results closer to the experimental binding energies for the smaller clusters without destroying the agreement for the larger clusters.

Though the calculated stepwise solvation energy provides a good first approximation to the stepwise spectral shifts, as we noted above, the experimental stepwise spectral shift also reflects changes to the vibrational frequencies of, particularly, the hydrogen atom bending modes on the neutral surface. This is not accounted for in the present study. In our investigation of scaled $Ar\cdot(IHI)^-$ potentials, we find little effect on the structure of the complexes. On the basis of this observation, we elect to use the potentials described above, which contain no adjustable parameters, for our initial investigations of the dynamics of the $Ar_n\cdot(IHI)^-$ complexes. When we include these quantum effects in the analysis, we will modify the potentials and expect we will be able to obtain good agreement with experiment over the entire range of cluster sizes.

C. Dynamics of $Ar_n\cdot(IHI)$. To investigate the dynamics of $Ar_n\cdot(IHI)$, we ran 7000 classical trajectories and analyzed the time dependence of the interiodine distance, R_{I-I}, as a function of the number of argon atoms. The results are plotted in Figure 4. In general, we find that the average rate of separation of the iodine atoms decreases with increasing n, with the exception of $n = 5$ where the rate of I−I separation increases when compared with $n = 4$. This exception can be explained in terms of a trapping of the hydrogen atom by the argon atoms. A similar effect was also observed in the dynamics of $Ar_n\cdot(ClHCl)$.[26] This effect, which is more pronounced for $n = 5$ and 6, causes an enhancement of the energy transfer between the hydrogen and the iodine atoms resulting in a faster separation of the iodine atoms. When more than six argon atoms are added to the system, they block the I−I dissociation, causing a slower dissociation of the IHI complex as the number of argon atoms is increased. This caging of IHI by the surrounding argon atoms becomes more pronounced for large values of n.

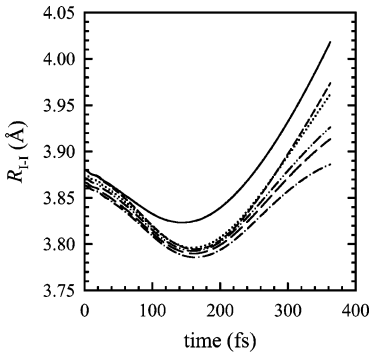

Figure 4. Plots of the time dependence of the average R_{I-I} for $n = 0$ (solid line), $n = 6$ (short dashed line), $n = 12$ (dotted line), $n = 13$ (dash−dot−dot line), $n = 19$ (long dashed line), and $n = 20$ (dash−dot line).

We further investigated the dynamics of $Ar_n\cdot(IHI)$ by focusing on the hydrogen atom. The results are shown in Figure 5 where we plot the Cartesian positions of the hydrogen atom at $t = 363$ fs (15 000 au) for each of 1000 trajectories. At $t = 0$ the hydrogen atom is located near the center of the I−I bond. After 363 fs, the distribution has spread and its shape depends on the positions of the argon atoms. When no argon atoms are present, the hydrogen atom is free to move away from the I−I axis, spreading around both of the iodine atoms, Figure 5a. This corresponds to the hydrogen atom orbiting around one of the iodine atoms and forming HI with nonzero angular momentum. Similar behavior was reported for the quantum dynamics of the ClHCl complexes.[26]

The introduction of one to four argon atoms limits the motion of the hydrogen atom, localizing the distribution of the hydrogen atoms at $t = 363$ fs in regions of configuration space where the argon atoms are not located. This is illustrated in Figure 5b for $n = 3$. Addition of a fifth and sixth argon atom causes a stronger localization of the hydrogen atom near the center of the complex, Figure 5c. For $n = 13$, the argon atoms prevent the hydrogen atom from moving around the more solvated iodine atom and for $n = 20$, Figure 5d, the argon atoms entirely block the orbiting motion of the hydrogen atom, confining it to the center of the I−H−I configuration.

The trapping of the hydrogen atom by the heavy atoms can be quantified by calculating the fraction of hydrogen atoms that are confined in the center of the I−I bond and dividing the remaining probability into fractions that are closer to each of the iodine atoms after 363 fs. This is illustrated in the inset of Figure 6. The plot in Figure 6 shows that for $n \leq 2$ there is a reduction in the fraction of hydrogen atoms that are trapped near the center of of the I−I bond. This is the result of a repulsive interaction between the hydrogen atom and the argon atoms that forces a larger fraction of the hydrogen atoms to move away from the center of the I−I bond. For $n = 3$ this behavior starts to reverse. This is due to the argon atoms limiting the available configuration space through which the hydrogen atom can escape from the center of the complex. When five and six argon atoms are added to IHI, a pronounced increase of the fraction of the hydrogen atoms that are trapped near the center of the I−I bond is observed. This is consistent with the observed faster separation of the iodine atoms for $n = 5$ and 6 when compared with the $n = 4$ case.

When more than six argon atoms are introduced, the fraction of the hydrogen atoms that remain near the center of the I−I bond continues to increase, whereas the fraction of the hydrogen atoms that are near to the more solvated iodine atom, I_2, decreases. This trend continues through $n = 14$. For larger

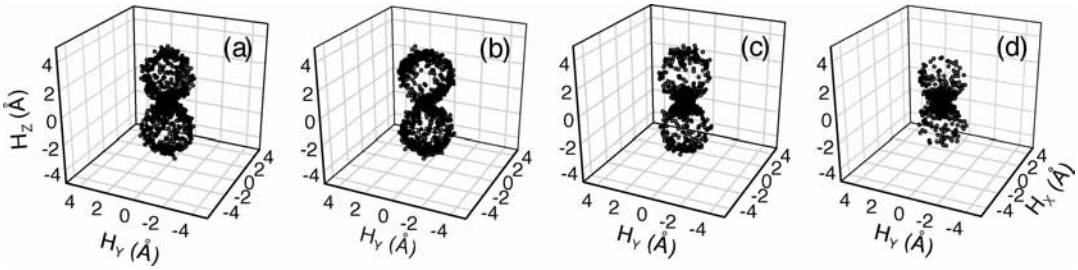

Figure 5. Plots of the Cartesian coordinates of the hydrogen atom at $t = 363$ fs when (a) $n = 0$, (b) $n = 3$, (c) $n = 6$, and (d) $n = 20$. These plots reflect the results of 1000 classical trajectories.

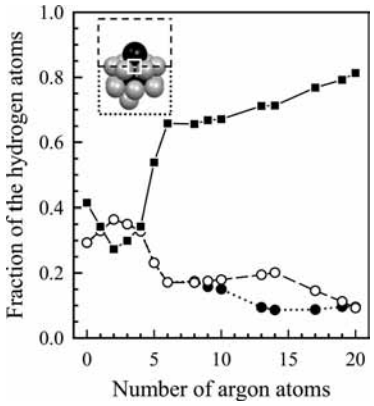

Figure 6. Plot of the fraction of the hydrogen atoms in each of the three regions, illustrated in the inset. The black squares show the fraction that is located inside a 8 Å^3 cube that is centered at the center of the I−I bond (indicated by a white square in the inset). The black circles and dotted line indicate the fraction of the hydrogen atoms that are outside of the cube and have $z < 0$. The dashed line and white circles show the fraction of the hydrogen atoms that are outside of the cube with $z > 0$.

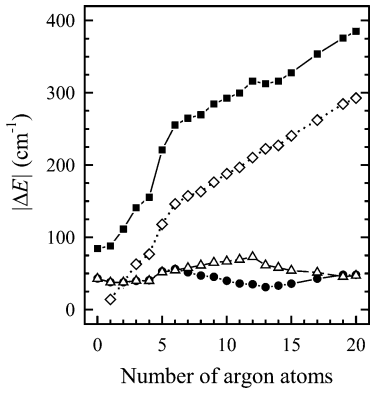

Figure 7. Plots of the average change in energy between $t = 0$ and 363 fs as a function of the number of argon atoms. The results for the hydrogen atom are plotted with black squares, I_1 with black circles, and I_2 with white triangles. The sum of the energy change for all of the argon atoms is plotted with white diamonds. It should be noted that in these simulations the hydrogen atom loses energy whereas the argon and iodine atoms gain energy.

clusters, the fraction of the hydrogen atoms that are nearer I_2 remains nearly constant. The fraction of hydrogen atoms that are nearer I_1 shows a slight increase up to $n = 14$ and a decrease for larger clusters. The above differences can be understood in terms of the positions of the argon atoms. The more argon atoms that are solvating a particular iodine atom, the less configuration space is available for the hydrogen atom to explore.

As a last step in our classical investigation, we analyze the energy transfer among the atoms. This is achieved by calculating the difference between the energies of each of the atoms at $t =$ 363 fs and $t = 0$. At time t the energy for a single atom is given by

$$E_i^t = T_i^t + V_i^t \tag{13}$$

where T_i^t is the kinetic energy of the atom i at time t and V_i^t is the potential energy of the atom i. Because the potential energy of a single atom is not a well-defined quantity we employ the following partitioning

$$V_{I_1} = \frac{m_{Ar}}{m_I + m_{Ar}} \sum_{i=1}^{n} V_{Ar-I}(R_{Ar_iI_1}) + \frac{m_H}{2(2m_I + m_H)} V_{IHI}$$

$$V_H = \frac{m_{Ar}}{m_H + m_{Ar}} \sum_{i=1}^{n} V_{Ar-H}(R_{Ar_iH}) + \frac{2m_I}{2m_I + m_H} V_{IHI}$$

$$V_{I_2} = \frac{m_{Ar}}{m_I + m_{Ar}} \sum_{i=1}^{n} V_{Ar-I}(R_{Ar_iI_2}) + \frac{m_H}{2(2m_I + m_H)} V_{IHI}$$

$$V_{Ar_i} = \frac{m_I}{m_I + m_{Ar}} [V_{Ar-I}(R_{Ar_iI_1}) + V_{Ar-I}(R_{Ar_iI_2})] + \frac{m_H}{m_H + m_{Ar}} V_{Ar-H}(R_{Ar_iH}) + \frac{1}{2} \sum_{j=1, j\neq i}^{n} V_{Ar-Ar}(R_{Ar_iAr_j}) \tag{14}$$

where m_I, m_H, and m_{Ar} are the masses of the iodine, hydrogen, and argon atoms, respectively, V_{Ar-I}, V_{Ar-H}, and V_{Ar-Ar} are the potentials given in eq 7, and V_{IHI} is the LEPS potential. As noted above, when the solvation is not symmetric, I_1 is the less solvated iodine atom. The average energy change for the hydrogen and iodine atoms after 363 fs is shown in Figure 7. In the same figure we also plot the sum of the energy change for all of the argon atoms after 363 fs. It should be noted that while the argon and iodine atoms gain energy over time, the hydrogen atom loses energy.

Figure 7 shows an increase in the energy lost from the hydrogen atom with increasing n. Most of the energy that is lost from the hydrogen atom is gained by the argon atoms. Examination of Figure 7 shows that the energy gained by the argon atoms increases monotonically with n. This increase is approximately linear for $n = 0-4$. For $n = 5$ a larger increase is observed and for $n \geq 6$ the increase in the energy gained by the argon becomes approximately linear again but the slope is smaller than that for the less solvated clusters. This behavior can be understood by considering the energy gained by the argon atoms in different binding positions. Because the first six argon atoms form a ring around the center of $(IHI)^-$, the hydrogen atom will interact most strongly with these argon atoms. This leads to a greater increase in the energy gained by the argon atoms for the smaller clusters compared to that for the larger clusters. In terms of the energy lost from the hydrogen atom,

Figure 7 shows an increase in slope between $n = 4$ and 5. This is consistent with the faster separation of the iodine atoms and the trapping of the hydrogen atom at these cluster sizes, discussed above. For $n = 12-14$ we find an almost constant energy loss from the hydrogen atom. As described above the 12th argon atom completes the second ring on $(IHI)^-$, the 13th one caps the more solvated end of the cluster, and the 14th argon atom starts a third ring on the less solvated iodine atom. Due to the symmetry of the clusters with six or fewer argon atoms we find that the same amount of energy is gained by both of the iodine atoms. When we break this symmetry by adding more argon atoms to the I_2 end of the complex, we find that I_2 gains more energy than I_1. If instead of comparing absolute energy differences, we had plotted the percentage change of the energy, we would have found nearly identical results for the two iodine atoms. We attribute the larger energy gain by the more solvated iodine atom to a larger initial energy, resulting from interactions with more of the argon atoms. Finally, we note that over the time scale of the simulations the clusters remain intact.

Summary and Conclusions

In this paper, we report the results of an investigation of the effects of argon atoms on the transition state dynamics of the I + HI reaction through an analysis of the $Ar_n \cdot (IHI)^-$ geometries and classical simulations of the dynamics of the $Ar_n \cdot (IHI)$ complexes. We find that as more argon atoms are introduced to the complex, they cluster around $(IHI)^-$, forming three six-atom rings that are perpendicular to the I−I axis. The first is formed around the hydrogen atom and the other two form around the iodine atoms, and the final two argon atoms cap the two ends of the cluster. Theoretical calculations performed by Adamovic and Gordon on the anion and comparisons between the calculated $\Delta E_{solv}(n)$ values and the experimental stepwise shifts measured from the $Ar_n \cdot (IHI)^-$ PE spectra support these results. Simulations of the dynamics of $Ar_n \cdot (IHI)$ show an overall decrease of the average rate of I−I separation with increasing cluster size. This is interpreted to reflect a caging of the hydrogen atom by the surrounding argon atoms.

Analysis of the hydrogen fractions at the center of the I−I bond and around the two iodine atoms show an increased trapping of the hydrogen atom near the center of the complex with increasing number of argon atoms. In addition, we observe an enhancement of the energy transfer between the hydrogen atom and the argon and iodine atoms with increasing n. Finally, due to the small amount of energy that is gained by the iodine and argon atoms when compared with the energy lost by the hydrogen atom and the small deviation of the argon atoms from their initial positions over the time scales of the simulations, we expect that a rigid cage approximation, where the hydrogen atom is allowed to move inside a cage formed by the iodine and argon atoms, might be fruitful as we investigate quantum effects in the $Ar_n \cdot (IHI)^-$ PE spectra.

Acknowledgment. We thank Professor Mark S. Gordon for sharing his results for these systems prior to publication and Dr. R. R. Lucchese for providing us with the codes to evaluate the Ar−HI potential. We also thank the National Science Foundation through Grant number CHE-0200968, the donors to the Petroleum Research Fund administered by the American Chemical Society, and the Dreyfus foundation awards program for partial support on this work.

References and Notes

(1) Steinfeld, J. I.; Francisco, J. S.; Hase, W. L. *Chemical Kinetics and Dynamics*, 2nd ed.; Prentice Hall: Upper Saddle River, NJ, 1999.
(2) Neumark, D. M. *Annu. Rev. Phys. Chem.* **1992**, *43*, 153.
(3) Brooks, P. R. *Chem. Rev.* **1988**, *88*, 407.
(4) Polanyi, J. C.; Zewail, A. H. *Acc. Chem. Res.* **1995**, *28*, 119.
(5) Metz, R. B.; Bradforth, S. E.; Neumark, D. M. *Adv. Chem. Phys.* **1992**, *81*, 1.
(6) Weaver, A.; Metz, R. B.; Bradforth, S. E.; Neumark, D. M. *J. Phys. Chem.* **1988**, *92*, 5558.
(7) Liu, Z.; Gómez, H.; Neumark, D. M. *Chem. Phys. Lett.* **2000**, *332*, 65.
(8) Liu, Z.; Gómez, H.; Neumark, D. M. *Faraday Discuss.* **2001**, *118*, 221.
(9) Waller, I. M.; Kitsopoulos, T. N.; Neumark, D. M. *J. Phys. Chem.* **1990**, *94*, 2240.
(10) Metz, R. B.; Weaver, A.; Bradforth, S. E.; Kitsopoulos, T. N.; Neumark, D. M. *J. Phys. Chem.* **1990**, *94*, 1377.
(11) Bradforth, S. E.; Weaver, A.; Arnold, D. W.; Metz, R. B.; Neumark, D. M. *J. Chem. Phys.* **1990**, *92*, 7205.
(12) Neumark, D. M. *Phys. Chem. Commun.* **2002**, *5*, 76.
(13) Schatz, G. C. *J. Chem. Phys.* **1989**, *90*, 4847.
(14) Schatz, G. C. *J. Phys. Chem.* **1990**, *94*, 6157.
(15) Schatz, G. C.; Sokolovski, D.; Connor, J. N. L. *Faraday Discuss. Chem. Soc.* **1991**, *91*, 17.
(16) Engel, V. *J. Chem. Phys.* **1991**, *94*, 16.
(17) Metz, R. B.; Neumark, D. M. *J. Chem. Phys.* **1992**, *97*, 962.
(18) Schatz, G. C.; Florance, S.; Lee, T. J.; Bauschlicher, C. W. *Chem. Phys. Lett.* **1993**, *202*, 495.
(19) Rougeau, N.; Marcotte, S.; Kubach, C. *J. Chem. Phys.* **1996**, *105*, 8653.
(20) Balint-Kurti, G. G.; Schatz, G. C. *J. Chem. Soc., Faraday Trans.* **1997**, *93*, 755.
(21) Takatsuka, K. *Phys. Rev. A* **1997**, *55*, 347.
(22) Kaledin, A.; Skokov, S.; Bowman, J. M.; Morokuma, K. *J. Chem. Phys.* **2000**, *113*, 9479.
(23) McCoy, A. B.; Gerber, R. B.; Ratner, M. A. *J. Chem. Phys.* **1994**, *101*, 1975.
(24) McCoy, A. B. *J. Chem. Phys.* **1995**, *103*, 986.
(25) McCoy A. B. In *Advances in Classical Trajectory Methods*; Hase W. L., Ed.; JAI Press Inc.: Greenwich, CT, 1998; Vol. 3, p 183.
(26) Lavender, H. B.; McCoy, A. B. *J. Phys. Chem. A* **2000**, *104*, 644.
(27) McIntosh, A.; Wang, Z.; Castillo-Chará, J.; Lucchese, R. R.; Bevan, J. W.; Suenram, R. D.; Legon, A. C. *J. Chem. Phys.* **1999**, *111*, 5764.
(28) Zhao, Y.; Yourshaw, I.; Reiser, G.; Arnold, C. C.; Neumark, D. M. *J. Chem. Phys.* **1994**, *101*, 6538.
(29) Aziz, R. A.; Slaman, M. J. *J. Chem. Phys.* **1990**, *92*, 1030.
(30) Burcl, R.; Cybulski, S. M.; Szczęśniak, M. M.; Chalasiński, G. *J. Chem. Phys.* **1995**, *103*, 299.
(31) Hutson, J. M. *J. Chem. Phys.* **1988**, *89*, 4550.
(32) Metz, R. B.; Neumark, D. M. *J. Chem. Phys.* **1992**, *97*, 962.
(33) Manz, J.; Römelt, J. *Chem. Phys. Lett.* **1981**, *81*, 179.
(34) Raff, L. M.; Thompson, D. L. In *Theory of Chemical Reaction Dynamics*; M. Baer., Ed.; CRC Press: Boca Raton, FL, 1985; Vol. 3, p 1.
(35) Wilson, E. B.; Decius, J. C.; Cross, P. C. *Molecular Vibrations*; Dover: New York, 1955.
(36) Allen, M. P.; Tildsley, D. J. *Computer Simulations of Liquids*; Oxford Science Publications: New York, 1987.
(37) Adamovic, I.; Gordon, M. S. *J. Phys. Chem. A* **2004**, *108*, 11042.
(38) Faeder, J.; Delaney, N.; Maslen, P. E.; Parson, R. *Chem. Phys. Lett.* **1997**, *270*, 196.
(39) Batista, V. S.; Coker, D. F. *J. Phys. Chem.* **1999**, *110*, 6583.
(40) Greenblatt, B. J.; Zanni, M. T.; Neumark, D. M. *J. Chem. Phys.* **1999**, *111*, 10566.
(41) Maslen, P. E.; Papanikolas, J. M.; Faeder, J.; Parson, R.; ONeil, S. V. *J. Chem. Phys.* **1994**, *101*, 5731.